29. K. Kasahara, http://cosmos.n.kanagawa-u.ac.jp/EPICSHome/.
30. M. Amenomori et al., Astrophys. J. 633, 1005 (2005).
31. F. A. Aharonian et al., A & A 393, L37 (2002).
32. S. D. Hunter et al., Astrophys. J. 481, 205 (1997).
33. R. Atkins et al., Phys. Rev. Lett. 95, 251103 (2005).
34. G. Walker, R. Atkins, D. Kieda, Astrophys. J. 614, L93 (2004).
35. L. Bergamasco et al., in Proc. 21th Int. Cosmic Ray Conf. (Adelaide), 6, 372–375 (1990).
36. E. N. Parker, Astrophys. J. 145, 811 (1966).
37. Z. H. Fan, Y.-Q. Lou, Nature 383, 800 (1996).
38. Y.-Q. Lou, Z. H. Fan, Mon. Not. R. Astron. Soc. 341, 909 (2003).
39. Y.-Q. Lou, X. N. Bai, Mon. Not. R. Astron. Soc., in press, astro-ph/0607328 (2006).
40. Unless otherwise stated, images in Figs. 1 to 4 are presented using pixels in a radius of 5° and are sampled over a square grid of side width 2°; the modal energy is 3 TeV.
41. The collaborative experiment of the Tibet Air Shower Arrays has been performed under the auspices of the Ministry of Science and Technology of China and the Ministry of Foreign Affairs of Japan. This work was supported in part by Grants-in-Aid for Scientific Research on Priority Areas (712) (MEXT), by the Japan Society for the Promotion of Science, by the National Natural Science Foundation of China, and by the Chinese Academy of Sciences. The authors thank J. Kóta for reading the manuscript and for critical comments.

REPORTS

Isolated Single-Cycle Attosecond Pulses

G. Sansone,[1] E. Benedetti,[1] F. Calegari,[1] C. Vozzi,[1] L. Avaldi,[2] R. Flammini,[2] L. Poletto,[3] P. Villoresi,[3] C. Altucci,[4] R. Velotta,[4] S. Stagira,[1] S. De Silvestri,[1] M. Nisoli[1]*

We generated single-cycle isolated attosecond pulses around ~36 electron volts using phase-stabilized 5-femtosecond driving pulses with a modulated polarization state. Using a complete temporal characterization technique, we demonstrated the compression of the generated pulses for as low as 130 attoseconds, corresponding to less than 1.2 optical cycles. Numerical simulations of the generation process show that the carrier-envelope phase of the attosecond pulses is stable. The availability of single-cycle isolated attosecond pulses opens the way to a new regime in ultrafast physics, in which the strong-field electron dynamics in atoms and molecules is driven by the electric field of the attosecond pulses rather than by their intensity profile.

The past decade has seen remarkable advances in the field of femtosecond (1 fs = 10^{-15} s) light pulses with few optical cycles (1). The main achievements have been (i) the generation of ultrabroadband light pulses, directly from a laser oscillator or with the use of external spectral broadening mechanisms; (ii) the development of sophisticated techniques for dispersion compensation on ultrabroad bandwidths; (iii) the use of experimental methods for complete temporal characterization of ultrashort pulses, particularly frequency-resolved optical gating (FROG) (2) and spectral phase interferometry for direct electric field reconstruction (SPIDER) (3), in a number of different experimental implementations; and (iv) the generation of few-cycle light pulses with precisely controlled and reproducible electric field waveform [stabilized carrier-envelope phase (CEP)] (4–6). We show that these achievements can now be extended to the attosecond (1 as = 10^{-18} s) domain. We demonstrate the compression and the complete temporal characterization of isolated pulses with durations down to 130 as at 36-eV photon energy, which consist of less than 1.2 periods of the central frequency. This source of extreme ultraviolet (XUV) radiation lends itself as a tool to investigate basic electron processes in a spectral range approaching the energy level of the outermost electrons in atoms, molecules, and solid-state systems. The XUV source opens the way to a new regime in the applications of attosecond pulses in which a medium interacts with nearly single-cycle isolated attosecond pulses. Moreover, in this case it is appropriate to analyze the role of the CEP of the generated attosecond pulses. Using numerical simulations, we demonstrate that the carrier-envelope phase of the attosecond pulses is characterized by an excellent stability.

So far, isolated attosecond pulses with multiple optical cycles have been produced by selecting the high-energy (cut-off) harmonics (~90 eV) generated in neon by few-cycle (<7 fs) linearly polarized fundamental pulses with stabilized CEP (7–9). In this case, the minimum pulse duration of the XUV pulses is limited by the bandwidth of the selected cut-off harmonics (~10 eV), thus preventing the generation of single-cycle attosecond pulses. A different approach for the generation of broadband isolated attosecond pulses is based on the use of phase-stabilized few-cycle driving pulses in combination with the polarization gating technique (10–13). Such a method uses the strong dependence of the harmonic generation process on the ellipticity of the driving pulses in order to obtain a temporal window of linear polarization for the fundamental pulses. XUV generation is possible only during this temporal polarization gate, which can be shorter than half an optical cycle of the fundamental radiation. In combination with the use of few-cycle driving pulses with stable CEP, this technique allows the generation of broadband isolated attosecond pulses. The advantages of this method are (i) the generation of broadband XUV pulses; (ii) the broad tunability of the attosecond pulses upon changing the generating gas medium; (iii) energy scalability; and (iv) the possibility to access the single-cycle regime.

The generation of broadband attosecond pulses is an important tool for photoelectron spectroscopy. Although they are not Fourier limited (chirped pulses), broadband attosecond pulses can be used to measure attosecond electron dynamics just as effectively as if the pulses were transform limited (14). However, in this case a complete temporal characterization of the attosecond pulses is required. On the other hand, for a number of applications in which the temporal structure of the attosecond pulses is important, dispersion compensation is required in order to obtain pulses with duration close to the transform-limited value. To completely characterize the attosecond pulses in terms of temporal intensity and phase, we experimentally applied the method of FROG for complete reconstruction of attosecond burst (FROG CRAB, hereafter called CRAB) (15), an extension to attosecond electron wavepackets of the FROG method. When an atom is ionized by an XUV attosecond electric field in the presence of a streaking infrared (IR) pulse, the IR electric field acts as an ultrafast phase modulator on the generated electron wavepacket. The corresponding photo-ionization spectrum can be written as a FROG spectrogram with a pure phase gate $\phi(t)$ (15):

$$\phi(t) = -\int_t^\infty dt'[\mathbf{v} \cdot \mathbf{A}(t') + \mathbf{A}^2(t')/2] \quad (1)$$

where $\mathbf{A}(t)$ is the vector potential of the IR field and $\mathbf{v}$ is the final electron velocity. A number of iterative algorithms can then be used to reconstruct the electric field of both the attosecond pulse and of the streaking IR pulse from the measured CRAB trace.

[1]National Laboratory for Ultrafast and Ultraintense Optical Science–CNR-Istituto Nazionale per la Fisica della Materia, Department of Physics, Politecnico, Piazza Leonardo da Vinci 32, 20133 Milano, Italy. [2]CNR-Istituto di Metodologie Inorganiche e dei Plasmi Area della Ricerca di Roma 1, Monterotondo Scalo 00016, Italy. [3]Laboratory for Ultraviolet and X-ray Optical Research–CNR-INFM, Department of Information Engineering–Università di Padova, Padova 35131, Italy. [4]Consorzio Nazionale Interuniversitario per le Scienze Fisiche della Materia-Dipartimento di Scienze Fisiche, Università di Napoli Federico II, Napoli 80138, Italy.

*To whom correspondence should be addressed. E-mail: mauro.nisoli@fisi.polimi.it

We adjusted the CEP of the driving few-cycle light pulses [full-width at intensity half-maximum (FWHM): $\tau_D = 5$ fs; central wavelength: $\lambda_D = 750$ nm] with controlled electric field in order to generate broadband and continuous XUV spectra in an Argon cell with static pressure, using the process of high-order harmonic generation (16, 17). The required temporal modulation of the driving IR pulse polarization was obtained with the use of two birefringent plates [for a detailed description of the experimental apparatus, see the supporting online material (SOM) text]. Upon changing the CEP of the driving pulses, a clear transition from two emission bursts to a single emission burst was observed in the spectral domain (13). Using a grazing incidence toroidal mirror, we focused the attosecond pulses into an Argon gas jet. The streaking IR beam was spatially overlapped with the XUV beam in the gas jet. The generated photoelectrons were collected within an acceptance angle of $\pm 2°$ around $\theta = 0$, where θ is the angle between **v** and the polarization direction of the IR field.

Figure 1A shows a portion of an experimental CRAB trace, which represents the evolution of the photoelectron spectra as a function of the temporal delay between the XUV and the streaking IR pulses. The measured trace follows the evolution of the vector potential, $\mathbf{A}(t)$, of the streaking pulse. The temporal structure of the attosecond pulses was retrieved using the principal-component generalized projection algorithm (PCGPA) (18). In the reconstructed temporal intensity profile and phase of the XUV pulses (Fig. 1B), the pulse duration was 280 as (the Fourier limit is ~100 as), and the almost parabolic phase indicates the presence of a predominant second-order dispersion, corresponding to a positive linear chirp $C \cong 42$ fs^{-2}. Such pulses correspond to only 2.5 optical cycles of the carrier frequency. The measured CRAB trace and the corresponding reconstruction of the XUV pulses clearly demonstrate the generation of isolated pulses, consistent with the measurement of a continuous XUV spectrum, with no clear evidences of harmonic peaks. The measured modulation of the width of the photoelectron spectrum was determined not only by the XUV pulse duration, but also by the chirp of the attosecond pulses (15). In our experimental conditions, the presence of positive chirp leads to a decrease of the electronic spectrum width (thus resulting in a spectral peak increase) in the temporal regions characterized by a negative slope of the vector potential, as clearly visible in Fig. 1A.

The measured positive chirp is intrinsic to the XUV generation process, because the harmonic emission time varies quasi-linearly with harmonic frequency (the spectral components at higher frequencies are emitted after those at lower frequencies) (19). As recently demonstrated in the case of trains of attosecond pulses (20), the positive chirp of the XUV radiation produced by
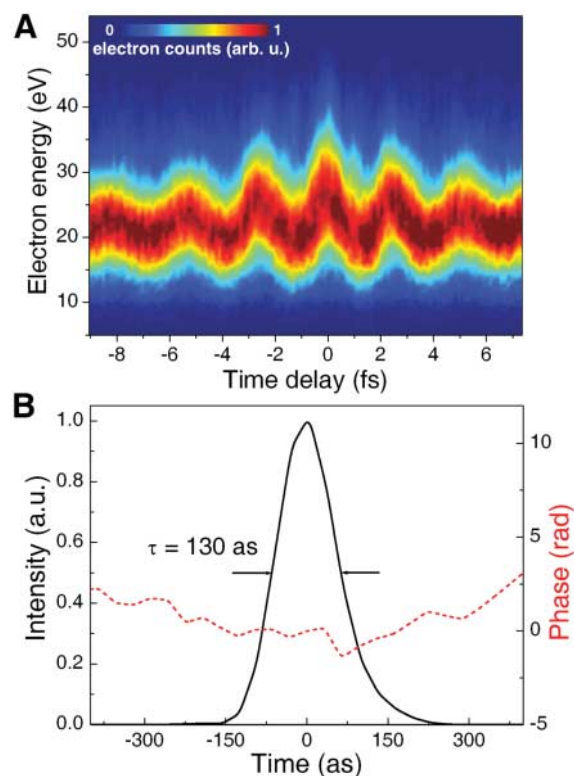
high-order harmonic generation can be compensated for by the negative group delay dispersion of thin aluminum foils, which is almost constant on the bandwidth of the generated attosecond pulses. The CRAB trace reported in Fig. 1A was measured using a 100-nm-thick aluminum foil (on a nickel mesh) on the XUV

Fig. 1. (**A**) Portion of an experimental CRAB trace measured in the case of a 100-nm-thick aluminum foil as a function of the temporal delay between the attosecond and the streaking IR pulses. Isolated attosecond pulses were generated by phase-stabilized, 5-fs pulses with modulated polarization state. (**B**) Reconstruction of the temporal intensity profile and phase of the attosecond pulses obtained from the CRAB trace after 5×10^4 iterations of the PCGPA algorithm.
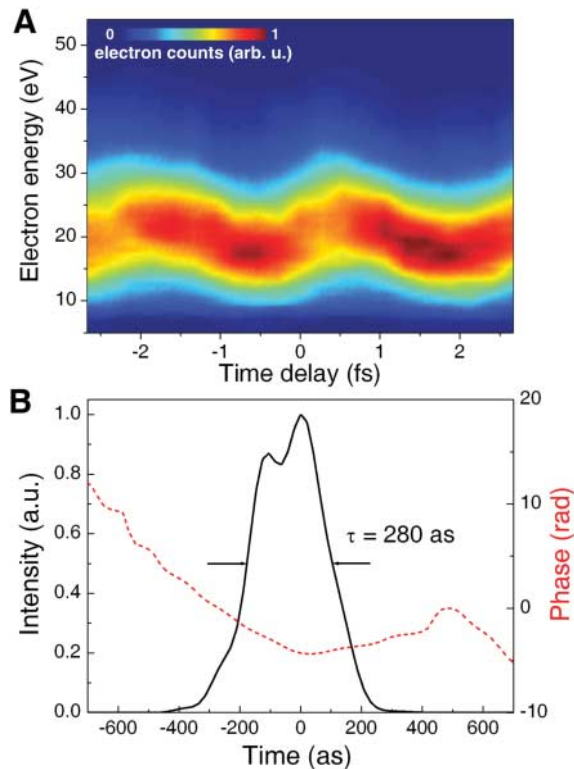
Fig. 2. (**A**) Complete experimental CRAB trace measured in the case of a 300-nm-thick aluminum foil as a function of the temporal delay between the attosecond and the streaking IR pulses. Isolated attosecond pulses were generated by phase-stabilized, 5-fs pulses with modulated polarization state. (**B**) Reconstruction of the temporal intensity profile and phase of the attosecond pulses obtained from the CRAB trace after 5×10^4 iterations of the PCGPA algorithm.

beam, in order to filter out the fundamental radiation, thus reducing the intrinsic positive chirp of the attosecond pulses. To test the possibility of further compressing the XUV pulses, we used thicker aluminum foils. Figure 2A shows a complete CRAB trace measured with a 300-nm-thick aluminum foil. The retrieved CRAB trace

(Fig. 3) reproduces the experimental trace: The CRAB error, evaluated as the root mean square error per element of the trace (*21*), is $\sim 10^{-3}$. In the intensity profile and the temporal phase of the retrieved attosecond pulses (Fig. 2B), the pulse duration (FWHM) is 130 as, close to the Fourier limit, thus indicating a good compensation of the intrinsic chirp. Such pulses correspond to fewer than 1.2 optical cycles of the carrier frequency (*22*).

The single-cycle nature of the generated isolated pulses has important implications for ultrafast science and adds another parameter to the study of attosecond phenomena: the carrier-envelope phase of the isolated attosecond pulses. To address this topic, we modeled the physical processes involved in the attosecond pulse generation using the nonadiabatic saddle-point method (*23*, *24*). Such an approach is based on the concept of Feynman's path integrals (*23*, *25*), which correspond to the complex trajectories (quantum paths) followed by the electrons from the ionization instant to the recombination with the parent ion in the process of high-order harmonic generation. We verified that the results of the numerical simulations were in agreement with the experimental data. In particular, they perfectly reproduce the effects of the CEP of the driving pulses on the spectral properties of the harmonic radiation. Moreover, the calculated temporal characteristics of the attosecond pulses (such as pulse duration, temporal and spectral phase, and chirp) turn out to be in very good agreement with the results of the experimental CRAB reconstruction procedure.

Figure 4 shows the electric field evolution calculated with the same driving pulse parameters that were used in the experiment and considering the contribution of the aluminum foil: The calculated pulse duration is 135 as (FWHM of the intensity profile), in agreement with the experimental result. The numerical simulations allow us to analyze the role of the experimental parameters on the CEP of the attosecond pulses. We calculated the temporal evolution of the XUV electric field upon changing the CEP of the driving pulses. We varied the driving CEP

values in a range of $\sim$175 mrad, giving rise to an efficient generation of isolated attosecond pulses. As demonstrated in Fig. 4, which displays the calculated electric field evolution for two different values of the CEP of the driving pulses, the CEP of the isolated attosecond pulses is negligibly influenced by variation of the CEP of the driving pulses. The two pulses reported in Fig. 4 were temporally shifted to overlap their intensity envelopes; the same shift determines the overlap of the electric fields of the corresponding driving pulses (*26*). In the considered CEP range of the IR pulses, only one electron quantum path contributes in a relevant way to the XUV emission. Because the corresponding electron wavepacket is emitted around a stationary point of the intensity profile of the driving pulse (*12*), relative changes of the emission and recombination times with respect to the IR intensity envelope (due to different CEP values) do not significantly affect the phase accumulated by the electron wavepacket (*27*). This determines an intrinsic mechanism for stabilization of the electric field of the attosecond pulses against variations of the CEP of the driving pulses. We have analyzed the effects of fluctuations of the excitation intensity; in this case, the induced variation of the attosecond CEP is very small. Indeed, a 2% intensity fluctuation leads to a $\sim$140-mrad CEP shift. The most important conclusion is that the CEP of the generated attosecond pulses is markedly stable. The attosecond CEP could be finely tuned, for example, by using aluminum foils with variable thickness: At 36 eV, a π CEP variation is induced by the addition of $\sim$80 nm of aluminum (although in this case also the pulse duration is affected).

The intrinsic robustness of the stability of attosecond pulse CEP should lead to new applications in ultrafast physics. These results pave the way to theoretical and experimental studies for the determination of the exact electric field evolution of attosecond XUV pulses. As the energy of the generated attosecond pulses can be easily increased by increasing the energy

of the IR driving pulses, we can envisage applications of the phase-stable single-cycle attosecond pulses to the study of strong-field electron dynamics in atoms and molecules, when processes are triggered and controlled by the electric field of the attosecond pulses, rather than by the intensity profile. As in the case of few-cycle IR pulses, we expect the possibility to influence and modify the ionization mechanisms of valence electrons upon changing the CEP of the attosecond pulses in the strong-field regime. In a lower intensity regime, as recently proposed in the case of few-cycle infrared pulses (*28*), the ultrafast dynamics of the population of bound and continuum states in atoms and molecules can be coherently influenced by the electric field temporal evolution of single-cycle attosecond pulses. The control of the CEP of such pulses provides an additional degree of freedom in the preparation and manipulation of atomic and molecular wavepackets. Another application is the investigation of photoionization processes in the presence of few-cycle XUV pulses and intense ($>10^{13}$ W/cm^2) synchronized IR fields. In this case, electron wavepackets can be emitted in the continuum following two different ionization channels: multiphoton above-threshold ionization associated to the IR field and absorption of single XUV photons. The coherent superposition of the two ionization probabilities determines an interference pattern in the photoelectron spectra, which should offer the possibility to measure the CEP of the attosecond pulses. Moreover, the availability of few-cycle isolated pulses in the photon energy range of about 30 eV is particularly important for the study of electron dynamics in chemistry and molecular and solid state physics, in which a number of fundamental processes are related to the outermost electrons, directly accessible by the generated attosecond pulses. On the other hand, the possibility of generating single-cycle pulses of less than 100 as at higher energy with the use of the polarization gating method in neon (*13*) should allow the study of the coherent dynamics of inner-shell electrons with unprecedented temporal resolution.
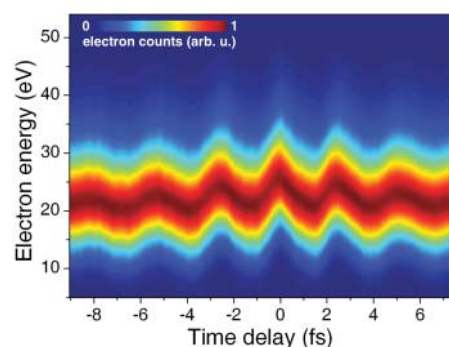
Fig. 3. Reconstruction of the CRAB trace of the attosecond pulses retrieved from the experimental trace shown in Fig. 2A, after 5×10^4 iterations of the PCGPA algorithm.
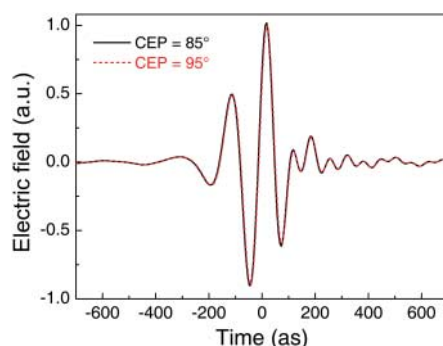
Fig. 4. Electric field of 135-as isolated pulses calculated for two different values of the CEP of the driving pulses with the use of the nonadiabatic saddle-point method. The simulations have been performed assuming the same driving pulse parameters that were used in the experiment.

References and Notes
1. U. Keller, *Nature* **424**, 831 (2003).
2. D. J. Kane, R. Trebino, *IEEE J. Quantum Electron.* **29**, 571 (1993).
3. C. Iaconis, I. A. Walmsley, *Opt. Lett.* **23**, 79 (1998).
4. A. Baltuška *et al.*, *Nature* **421**, 611 (2003).
5. E. Goulielmakis *et al.*, *Science* **305**, 1267 (2004).
6. E. Gagnon *et al.*, *Opt. Lett.* **31**, 1866 (2006).
7. M. Hentschel *et al.*, *Nature* **414**, 509 (2001).
8. R. Kienberger *et al.*, *Nature* **427**, 817 (2004).
9. I. P. Christov, M. M. Murnane, H. Kapteyn, *Phys. Rev. Lett.* **78**, 1251 (1997).
10. P. B. Corkum, N. H. Burnett, M. Y. Ivanov, *Opt. Lett.* **19**, 1870 (1994).
11. C. Altucci *et al.*, *Phys. Rev. A* **58**, 3934 (1998).
12. O. Tckerbakoff, E. Mével, D. Descamps, J. Plumridge, E. Constant, *Phys. Rev. A* **68**, 043804 (2003).
13. I. J. Sola *et al.*, *Nature Physics* **2**, 319 (2006).
14. G. L. Yudin, A. D. Bandrauk, P. B. Corkum, *Phys. Rev. Lett.* **96**, 063002 (2006).
15. Y. Mairesse, F. Quéré, *Phys. Rev. A* **71**, 011401(R) (2005).

16. A. L'Huillier, P. Balcou, *Phys. Rev. Lett.* **70**, 774 (1993).
17. J. J. Macklin, J. D. Kmetec, C. L. Gordon III, *Phys. Rev. Lett.* **70**, 766 (1993).
18. D. Kane, *IEEE J. Quantum Electron.* **35**, 421 (1999).
19. Y. Mairesse *et al.*, *Science* **302**, 1540 (2003).
20. R. López-Martens *et al.*, *Phys. Rev. Lett.* **94**, 033001 (2005).
21. K. W. DeLong, D. N. Fittinghoff, R. Trebino, *IEEE J. Quantum Electron.* **32**, 1253 (1996).
22. The maximum energy shift of the photoelectron spectra induced by the streaking IR pulse (~8 eV) is comparable to the photoelectron bandwidth, thus confirming that the phase modulation imposed by the streaking pulse is fast enough to warrant a correct characterization of the electron wavepacket generated by the XUV pulses.

23. M. Lewenstein, P. Balcou, M. Y. Ivanov, A. L'Huillier, P. B. Corkum, *Phys. Rev. A.* **49**, 2117 (1994).
24. G. Sansone, C. Vozzi, S. Stagira, M. Nisoli, *Phys. Rev. A.* **70**, 013411 (2004).
25. P. Salières *et al.*, *Science* **292**, 902 (2001).
26. The CRAB technique is not sensitive to the CEP of the attosecond pulses.
27. The accumulated phase is proportional to the ponderomotive energy, given by $U_P = E_D^2/4\omega_D^2$ (atomic units), where E_D is the electric field of the driving laser and ω_D is the fundamental angular frequency.
28. T. Nakajima, S. Watanabe, *Phys. Rev. Lett.* **96**, 213001 (2006).
29. This work was partially supported by the Marie Curie Research Training Network Ultrashort XUV Pulses for Time-Resolved and Nonlinear Applications (XTRA) (grant no. MRTN-CT-2003-505138), by Ministero dell'Università e della Ricerca under project Processi fisici nel dominio degli attosecondi and by Consiglio Nazionale delle Ricerche (CNR) under project Sorgente Pulsata e Amplificata di Radiazione Coerente.

Molecular Imaging Using a Targeted Magnetic Resonance Hyperpolarized Biosensor

Leif Schröder,[1,2] Thomas J. Lowery,[1,3] Christian Hilty,[1,2] David E. Wemmer,[1,3]* Alexander Pines[1,2]*

A magnetic resonance approach is presented that enables high-sensitivity, high-contrast molecular imaging by exploiting xenon biosensors. These sensors link xenon atoms to specific biomolecular targets, coupling the high sensitivity of hyperpolarized nuclei with the specificity of biochemical interactions. We demonstrated spatial resolution of a specific target protein in vitro at micromolar concentration, with a readout scheme that reduces the required acquisition time by >3300-fold relative to direct detection. This technique uses the signal of free hyperpolarized xenon to dramatically amplify the sensor signal via chemical exchange saturation transfer (CEST). Because it is ~10,000 times more sensitive than previous CEST methods and other molecular magnetic resonance imaging techniques, it marks a critical step toward the application of xenon biosensors as selective contrast agents in biomedical applications.

Magnetic resonance imaging (MRI) is established as a powerful method for tomography of opaque biological samples (*1*). However, its application in molecular imaging (determining the spatial distribution of specific molecules of interest) has been limited because of inherent low sensitivity (*2*). Conventional MRI techniques usually detect highly abundant nuclei, such as protons (^{1}H) of water (110 M ^{1}H concentration) and/or fat, to guarantee sufficient signal intensity despite the low thermal polarization. Contrast agents, including some that bind to specific biomolecular targets, have been developed that induce small but detectable changes in these strong signals. However, the required contrast agent concentration is ~0.5 to 2 mM for signal changes based on relaxation enhancements (*2*) or saturation transfer experiments (*3*). Application of exogenous ^{129}Xe circumvents limitations in sensitivity and contrast, because Xe nuclei can be hyperpolarized before transfer into the system of interest and their nuclear magnetic resonance (NMR) frequencies are extremely sensitive to the molecular environment.

Hyperpolarization amplifies the available magnetization by a factor of >10^4, and it is currently used to increase anatomical contrast in MRI for imaging of void spaces such as the lung (*4*).

Detection of specific biomolecules in a solution environment can be accomplished by xenon biosensors, which trap Xe atoms in molecular cages that have been functionalized to bind the desired target (*5*, *6*). Xenon biosensors are composed of a cryptophane-A cage (*7*), a linker, and a targeting moiety (Fig. 1A), which can be an antibody or ligand that enables detection of a specific analyte. The cage-encapsulated xenon nuclei give rise to a unique signal that is well shifted from that of free Xe. Hence, these compounds act as selective imaging contrast agents for near-zero background MRI that benefit from the high specificity of biochemical targeting (*5*, *6*). The excellent resolution of free and biosensor-bound Xe was used recently to obtain a one-dimensional NMR profile from a bead-immobilized biosensor in a perfusion phantom that delivers Xe-saturated water to a test volume inside the NMR probe (*8*). This setup mimics in principle Xe delivery to a biosensor-labeled volume of interest as it would be provided by the blood stream in vivo after injection or inhalation. Direct application of the xenon biosensor to molecular imaging has been impaired by the fact that, for typical experiments, only ~1% of dissolved Xe is associated with the sensor (*9*). A further challenge was shown to lie in the broadening of sensor signal in heterogeneous samples (*8*, *9*), leading to a significant reduction in signal to noise.

Here, we introduce a different approach for obtaining MR images of Xe biosensors that is based on chemical exchange between the biosensor-encapsulated Xe and the easily detectable pool of free Xe (*10*), thus making optimized use of the available biosensor-associated magnetization. These Xe nuclei fulfill the conditions of slow exchange on the NMR time scale; that is, the frequency difference of the resonances ($\Delta\omega$) is large compared with the exchange rate (τ_{ex}^{-1}) between the two sites: $\Delta\omega \gg \tau_{ex}^{-1}$. Such exchange is used for signal amplification by measuring a decrease in the intense free xenon signal after selective saturation of the biosensor-bound xenon. Exchange-mediated depletion of the free xenon signal requires that the exchange rate be fast compared with the longitudinal relaxation time of free xenon ($\tau_{ex}^{-1} \gg T_1^{-1}$) and that the saturation be effective (transition rate $W \geq \tau_{ex}^{-1}$). With a value of $T_1 \approx 66$ s in water (*11*) at 9.4 T and exchange dynamics characterized by $\tau_{ex} \approx 40$ ms (*10*), Xe nuclei in the sensor cages are ideal for saturation transfer.

The applied technique is similar to chemical exchange saturation transfer or CEST (*12*), which was previously developed for use with proton contrast agents. However, because the method presented here, HYPER-CEST, uses hyperpolarized nuclei with a long relaxation time, nearly the entire sensor-related magnetization depletion is stored in the observed signal.

This scheme allows substantial sensitivity improvement, which we demonstrated with two-dimensional images that were obtained in a few minutes of a biosensor solution sample with ~5 µM concentration of a recently described biosensor construct (*8*, *9*) that binds via its biotin moiety to avidin-functionalized agarose beads in an aqueous environment. The ^{129}Xe NMR spectra of such bead samples were composed of three different signals (Fig. 1A): free Xe in the bead medium resonates at $\delta_1 = 193.6$ parts per million (ppm) (referred to as "bead signal" in the following), free Xe in pure water at $\delta_2 = 192.5$ ppm, and Xe inside the biosensor cage at $\delta_3 = 65.4$ ppm (chemical shifts are

[1]Department of Chemistry, University of California, Berkeley, CA 94720, USA. [2]Materials Sciences Division, [3]Physical Biosciences Division, Lawrence Berkeley National Laboratory, Berkeley, CA 94720, USA.

*To whom correspondence should be addressed. E-mail: dewemmer@lbl.gov (D.E.W.); pines@berkeley.edu (A.P.)

Science

Isolated Single-Cycle Attosecond Pulses

G. Sansone, E. Benedetti, F. Calegari, C. Vozzi, L. Avaldi, R. Flammini, L. Poletto, P. Villoresi, C. Altucci, R. Velotta, S. Stagira, S. De Silvestri, and M. Nisoli

View the article online
https://www.science.org/doi/10.1126/science.1132838
Permissions
https://www.science.org/help/reprints-and-permissions

Use of this article is subject to the Terms of service